Author Manuscript

Published in final edited form as:

J Biomech. 2017 Feb 8;52:169-175.

Doi: 10.1016/j.jbiomech.2016.12.011.

Title:

Strain shielding in distal radius after wrist arthroplasty with a current generation implant: An in vitro analysis

Completo A[1], Pereira J[1], Nascimento A[2], Almeida F[2]

[1] Mechanical Engineering Department, University of Aveiro, Portugal

[2] Orthopaedics Department, Coimbra University Hospital, Portugal

ABSTRACT

A systematic review of peer reviewed articles has shown that the main cause for wrist arthroplasty revision is carpal and radial prosthetic loosening and instability. To improve arthroplasty outcomes, successive generations of implants have been developed over time. The problem with the current generation of implants is the lack of long-term outcomes data. The aim of the present work was to test the hypothesis that the current generation Maestro WRS implant has a stress, strain and stability behaviour which may be associated with a reduced risk of long-term radial component loosening. This study was performed using synthetic radii to experimentally predict the cortex strain behaviour and implant stability considering different load conditions for both intact and implanted conditions. Finite element models were developed to assess the structural behaviour of cancellous-bone and bone-cement, these models were validated against experimentally measured cortex strains. Measured cortex strains showed a significant reduction between intact and implanted states. Cancellous bone adjacent to the radial body component suffers a two to threefold strain reduction, comparing with the intact condition, while along the radial stem, in the axial direction, a strain increase was observed. It is concluded that the use of contemporary Maestro WRS implant changes the biomechanical behaviour of the radius and is associated with a potential risk of bone resorption by stress-shielding in the distal radius region for wrist loads in the range of daily activities.

Keywords: experimental strains; finite element model; radial component; stress-shielding

INTRODUCTION

Arthroplasty of the radiocarpal joint is performed much less commonly than identical surgeries on many other joints. Alternative treatments are in general perceived to be a better option in the wrist. Total fusion has historically demonstrated success as a treatment for alleviating pain from severe arthritis (Ilan and Retting, 2003), however, this solution results in significant loss of hand function (Weiss et al. 1995; Adey et al. 2005). Radiocarpal arthroplasty has been shown to preserve range of motion but the outcomes of early implants were not as favourable as those observed for arthroplasties performed in other joints (Minami et al. 2004; Radmer et al. 2003; Cooney et al. 2012). A systematic review of peer reviewed articles has shown that the main cause for revision is carpal and radial prosthetic loosening and instability (Cooney et al. 1984; Rahimtoola and Rozing 2003; Krukhaug et al. 2011). In order to improve radiocarpal arthroplasty outcomes, successive generations of implants have been developed (Cooney et al., 1984; Krukhaug et al. 2011; Boeckstyns et al., 2013; Nair, 2014). The problem with present generation of implants is the unavailability of data regarding long-term outcomes (Dellacqua, 2009; Boeckstyns et al., 2013; Nydick et al., 2012; Gaspar et al., 2016). Probably the best source of information is the Norwegian registry, however, none of the prostheses with long-term follow-up are currently being used.

It is hypothesized, that the present generation Maestro WRS implant, has a stress, strain and stability behaviour which may be associated with a reduced risk of radial component loosening in the long-term. Ideally, bone strain values should be low enough to avoid exceeding fatigue levels of materials, but also, must not be below strain-shielding inductive levels, which lead to significant bone atrophy, ultimately resulting in implant loosening. This study uses synthetic radii to experimentally predict cortex strain behaviour and implant stability for different load conditions. In addition, finite element (FE) models were developed to assess the structural behaviour of cancellous-bone and

bone-cement around the implant, these models were validated against experimentally measured cortex strains.

MATERIALS AND METHODS

Five synthetic radii (4th generation, left, model 3407, from Pacific Research Labs, WA, USA) were selected and used in the experimental study. Seven triaxial strain gauges (KFG-3-120-D17-11L3M2S, Kyowa, Japan) were glued on the thumb (Thu_D, Thu_P), dorsal (Dor_Dl, Dor_Dm, Dor_P) and palmar (Pal_D, Pal_P) sides of the radius cortex at two levels of the articular surface before prosthesis insertion (Figure 1). A reference axis was marked on the outer cortical surface to allow reproducible positioning of the strain gauges. The positions of the strain gauges were measured using a 3D coordinate measuring machine (Maxim, Aberlink, UK). The radial component of the Maestro™ WRS prosthesis (Biomet, Warsaw, IN, USA) was implanted into the radius by an experienced surgeon (Figure 2), according to the protocol described for this prosthesis. After radial broaching, bone-cement CMW-1 (DePuy, Warsaw, IN, USA) was injected into the cavity to fix the radial stem. Applied loads were obtained from the bibliography, as reasonable estimates of radiocarpal joint loads were obtained from theoretical and experimental studies (Swanson et al. 1970; Palmer and Werner, 1984: Schuind et al., 1995; Chadwick and Nicol, 2000). Three experimental load-cases were applied, which result from three radiocarpal joint reaction force alignments (θ) measured from the frontal plane (abduction $\theta = 15^{o}$, neutral $\theta = 0^{o}$ and adduction $\theta = 45^{o}$) with a magnitude of 350N, which is a force level that can be experienced during a grasp of approximately 25N (Schuind et al., 1995; Troy et al., 2013). The radius proximal region was rigidly fixed (Figure 2). In order to establish correlations with FE models and evaluate the risk of failure or resorption of the supporting cortex, the maximum-$\varepsilon 1$ and minimum-$\varepsilon 2$ principal strains within the plane of the gauge were calculated and averaged, and the standard deviations determined. Normal distribution of all data was evaluated through an

exploratory data analysis. Paired t-tests were performed to assess the statistical significant difference of the mean principal strains. The initial radial component stability was evaluated after 25,000 load cycles at a frequency of 1Hz through a pull-out force of 200N applied at the radial head (Shimadzu AGS-10KnXD). Implant mobility was evaluated through the analysis of force-displacement curves and visual check in order to identify some slippage/release of the implant.

Finite element analysis

Finite element (FE) models of intact and implanted radii were made from CT-scans of the experimental models, which were then converted to 3D models with an image processing software package (ScanIP, Simpleware Ltd. Exeter, UK). The implant models were created with a CAD modelling package (Catia, Dassault-Systèms, France). The FE meshes were built from 10-node second-order tetrahedral elements (C3D10). The number of elements were chosen based on convergence tests performed based on the maximal displacement and the minimal principal strains at 3 locations (thumb, dorsal and palmar sides) for the intact radius model. The convergence rate of the displacements was less than 0.5% and less than 4% for the minimal principal strains when nearly 112000 elements were used. Non-linear contact formulation analysis was performed with ABAQUS (6.12-1) (Providence, USA). The cement-radial-stem and bone-radial-body interfaces were modelled with a finite sliding surface-to-surface contact algorithm with a coefficient of friction of 0.25 (Mann et al., 1991) and 0.8 (Grant et al., 2007; Tajdari and Javadi 2006) respectively. The bone-cement assembly was considered rigidly bonded to the bone. The material properties used were those described by the manufacturer (Table 1) and were assumed to be homogeneous, isotropic and linear elastic. Regression analyses between the principal strains predicted by the FE models and experimentally measured strains were performed. The overall absolute difference between numerical and experimental cortex strains, the root-mean-square-error was calculated and expressed as a percentage of the peak values of the measured principal strains (RMSE %). The same

load-cases, were used to analyse principal cancellous bone strains, before and after implantation, as well as von Mises stresses in the bone-cement. The volume of bone-cement with stress values greater than the bone-cement fatigue limit was also determined.

RESULTS

The means and standard deviations of the cortex principal strains for each strain gauge are depicted in Figure_3 for abduction ($\theta = 15^o$), neutral ($\theta = 0^o$) and adduction ($\theta = 45^o$) load cases. The average standard deviation of the principal strain was less than 12%. Abduction and neutral load cases presented very similar cortex strain behaviour. The adduction load case presented the highest principal strains of all three load cases analysed. Excluding the distal dorsal strain gauges (Dor_Dl, Dor_Dm) the magnitude of minimal principal strain was greater than maximal principal strains, with the highest values measured on the most proximal strain gauge (Thu_P). Significant maximum and minimum principal cortex strain reductions ($p<0.05$) between intact and implanted states were observed in all strain gauges for all load cases (Table 2). After 25,000 load cycles (1Hz) the radial component presented good stability without any sign of slippage/release during the pull-out force. The linear regression correlation value (R^2) was 0.94 and the slope was 1.00 (Figure_4). The overall absolute difference between numerical and experimental cortex strains (RMSE %) was 14%. Figure_5 shows the patterns of the minimum principal strains in cancellous bone obtained in the FE analysis. For all load cases the implanted state increased three to four times cancellous-bone strains in the radial stem tip region comparing with the intact model. In the distal radius region, comparing with intact state, a two to threefold decrease is observed in cancellous bone strain around the radial body for abduction and neutral load cases. The highest bone-cement stress was reached in the adduction load case with 5.67 MPa, which represents an increase of 40% in relation to the abduction and neutral load cases (Table 3).

DISCUSSION

The aim of the present work was to investigate in-vitro implant–bone load transfer mechanisms and monitoring the radial strain shielding effect with the current generation Maestro wrist implant. To the authors' knowledge there are no other studies comparing stress-strain levels in intact and implanted wrists with a Maestro WRS implant, neither in-vitro nor using the FE method. The standard deviations of the measured cortex strains were within the range of those found in the literature which used other synthetic bones (Completo et al., 2007; Completo et al., 2010, Meireles et al., 2010). The average of the cortex principal strains in the implanted radius presented a significant reduction ($p<0.05$) relatively to the intact radius. The biological control mechanisms that produce the effect described by Wolff's law are poorly understood, but what is known is that in situations where bone loads are reduced or eliminated, bone mass is reabsorbed (Gross and Rubin 1995; Frost, 2003). These experimental results show that the distal radius is not immune to problems using the Maestro WRS implant. The FE models developed to analyse cancellous bone presented correlation, slope, intercept values of the linear regressions and RMSE values in the range of other previous experimental-numerical studies performed with synthetic bones (Completo et al., 2007; Heiner and Rubin, 2008) which reveals a good agreement between FE and measured strains. Cancellous bone strain behaviour in the intact radius was very similar for all load-cases analysed. In the implanted case, the distal region adjacent to the radial body component, suffers a strain reduction (two to three times) comparing with the intact condition. This decrease was accompanied with an axial direction strain increase along the radial stem, with peak strains at the radial stem tip region. Strain reduction around the distal region of the radial body component was slightly larger than those measured in the cortex, which may point to a risk of cancellous bone resorption for loads in the range of daily activities. In the cement around the radial stem, maximum stress values were reached at the tip, however the volume of cement above the fatigue limits for all load-cases studied (Huiskes 1993) was null. Some FE

studies found in the literature were developed in order to analyse the load distribution throughout wrist bones (Ulrich et al., 1999; Pistoia et al., 2002; Gislason et al., 2009; Bajuri eta al., 2012; Mueller et al., 2011; Guo et al., 2009), however, only one analysed an implanted wrist (Bajuri et al., 2013). As in the present study, a stress reduction was observed in the distal radius with the ReMotion (Small Bone Innovations) prosthesis. Bajuri et al. 2013, did not evaluate the cancellous bone behaviour adjacent to the ReMotion implant and concluded that normal healthy state cortex stress levels are not restored in the implanted model.

As in all experimental-numerical studies, the present study had some shortcomings, one such limitation is concerned with the use of synthetic bones and experimental simplifications required to represent the functioning Maestro wrist prosthesis. The advantage of using artificial bones is that specimen geometry is constant, which optimizes the reproducibility of results obtained in tests.

Experimental load-cases were simplified in terms of applied loads and structural links (ligaments, muscles, etc.), however, applied load-cases are representative of major loads acting upon the implant and bone structure, furthermore, due to the comparative nature of the study, it is concluded that the observed strain results are representative of major differences between intact and implanted states.

The main insight given by the present study is that the use of the current generation Maestro WRS prostheses changes the magnitude of bone strains (manifold) between intact and implanted states. Therefore, there is a potential risk of bone atrophy in the mid to long term due to the strain reduction around the distal region of radial body for loads in the range of daily wrist activities. These results contradict the initial hypothesis which stated that the present generation of Maestro WRS prostheses would be associated with a reduced risk of radial component loosening in the long-term.

Acknowledgements

The authors wish to thank: Program COMPETE funding through the projects POCI-01-0145-FEDER-016574, PTDC/EMS-TEC/3263/2014 and Projecto 3599 – PPCDT e comparticipado pelo Fundo Comunitário Europeu FEDER.

Conflict of interest statement

All of the above mentioned authors were involved in this study and preparation of manuscript. None of the herein presented material has been submitted for publication of any form elsewhere. None of the authors or institutions involved in this study has any vested interest that may conflict with carrying out this work in an independent manner.

REFERENCES

Adey, L., Ring, D., Jupiter, J.B., 2005. Health status after total wrist arthrodesis for posttraumatic arthritis. J Hand Surg [Am]. 30, 932-36.

Bajuri, M.N., Kadir, M.R., Raman, M.M., Kamarul, T., 2012. Mechanical and functional assessment of the wrist affected by rheumatoid arthritis: A finite element analysis. Med Eng Phys. 34, 1294-1302.

Bajuri, M.N., Abdul Kadir, M.R., Murali, M.R., Kamarul, T., 2013. Biomechanical analysis of the wrist arthroplasty in rheumatoid arthritis: a finite element analysis. Med Biol Eng Comput. 51, 175-186.

Boeckstyns, M.E., Herzberg, G., Sørensen, A.I., Axelsson, P., Krøner, K., Liverneaux, P.A., Obert, L., Merser, S., 2013. Can total wrist arthroplasty be an option in the treatment of the severely destroyed posttraumatic wrist? J Wrist Surg. 2, 324-29.

Chadwick, E.K., Nicol, A.C., 2000. Elbow and wrist joint contact forces during occupational pick and place activities. J Biomech. 33, 591-600.

Completo, A., Fonseca, F., Simões, J. A., 2007. "Experimental Evaluation of Strain Shielding in Distal Femur in Revision TKA", Experimental Mechanics 48, 817-824.

Completo, A., Fonseca, F., Simões, J. A., 2007. ”Experimental validation of the intact and implanted distal femur models”, J Biomech 40, 2467-76.

Completo, A., Rego, A., Fonseca, F., Ramos, A., Relvas, C., Simões, J.A., 2010. Biomechanical evaluation of proximal tibia behaviour with the use of femoral stems in revision TKA: an in vitro and finite element analysis. Clin Biomech. 25, 159-65.

Completo, A., Pereira, J., Fonseca, F., Ramos, A., Relvas, C., Simões, J., 2011. Biomechanical analysis of total elbow replacement with unlinked iBP prosthesis: an in vitro and finite element analysis. Clin Biomech. 26, 990-97.

Cooney, W., Beckenbaugh, R.D., Linscheid, R.L., 1984. Total wrist arthroplasty. Problems with implant failures. Clin Orthop Relat Res. 187, 121–28.

Cooney, W., Manuel, J., Froelich, J., Rizzo, M., 2012. Total wrist replacement: a retrospective comparative study. J Wrist Surg. 1, 165-72.

Dellacqua, D., 2009. Total Wrist Arthroplasty. Techniques in Orthopaedics. 24, 49-57.

Frost, H.M., 2003. Bone's mechanostat: a 2003 update. Anat Rec A Discov Mol Cell Evol Biol. 275, 1081-101.

Gaspar, M.P., Lou, J., Kane, P.M., Jacoby, S.M., Osterman, A.L., Culp, R.W., 2016. Complications Following Partial and Total Wrist Arthroplasty: A Single-Center Retrospective Review. J Hand Surg Am. 41, 47-53.

Gislason, M.K., Nash, D.H., Nicol, A., Kanellopoulos, A., Bransby-Zachary, M., Hems, T., Condon, B., Stansfield, B., 2009. A three-dimensional finite element model of maximal grip loading in the human wrist. Proceedings of the Institution of Mechanical Engineers, Part H: Journal of Engineering in Medicine. 223, 849–61.

Grant, J.A., Bishop, N.E., Götzen, N., Sprecher, C., Honl, M., Morlock, M.M., 2007. Artificial composite bone as a model of human trabecular bone: the implant-bone interface. J Biomech. ;40, 1158-64.

Gross, T.S., Rubin, C.T., 1995. Uniformity of resorptive bone loss induced by disuse. J Orthop Res. 13, 708-14.

Guo, X., Fan, Y., Li, Z.M., 2009. Effects of dividing the transverse carpal ligament on the mechanical behavior of the carpal bones under axial compressive load: a finite element study. Med Eng Phys. 31, 188-194.

Heiner, A., 2008. Structural properties of fourth-generation composite femurs and tibias. J. Biomech. 41, 3282–3284.

Huiskes, R., 1993. Mechanical failure in total hip arthroplasty with cement. Curr. Orthop.7, 239-47.

Ilan, D.I., and Rettig, M.E.,2003. Rheumatoid arthritis of the wrist. Bull Hosp Jt Dis. 61, 179-85.

Krukhaug, Y., Lie, S.A., Havelin, L.I., Furnes, O., Hove, L.M., 2011. Results of 189 wrist replacements. A report from the Norwegian Arthroplasty Register. Acta Orthop. 82, 405-09.

Mann, K.A., Bartel, D.L., Wright, T.M., 1991. Ingraffe AR. Mechanical characteristics of the stem-cement interface. J Orthop Res. 9, 798-808.

Meireles, S., Completo, A., Simões, J., Flores P., 2010. Strain shielding in distal femur after patellofemoral arthroplasty under different activity conditions. J Biomech. 43, 477-84.

Minami, M., Kato, S., Hirachi, K., Nagai, M., 2004. A total wrist arthroplasty in rheumatoid arthritis: a case followed for 24 years. Mod Rheumatol. 14, 488-93.

Mueller, T.L., Christen, D., Sandercott, S., Boyd, S.K., van Rietbergen, B., Eckstein, F., Lochmüller, E.M., Müller, R., van Lenthe, G.H., 2011. Computational finite element bone mechanics accurately predicts mechanical competence in the human radius of an elderly population. Bone. 48, 1232 38.

Nair, R., 2014. Review Article: Total wrist arthroplasty. Journal of Orthopaedic Surgery. 22, 399-405.

Nydick, .JA., Greenberg, S.M., Stone, J.D., Williams, B., Polikandriotis, J.A., Hess, A.V., 2012. Clinical outcomes of total wrist arthroplasty. J Hand Surg Am. 37, 1580-84.

Palmer, A., Werner, F., 1984. Biomechanics of the distal radioulnar joint. Clin Orthop Relat Res. 187, 26–35.

Pistoia, W., van Rietbergen, B., Lochmüller, E.M., Lill, C.A., Eckstein, F., Rüegsegger, P., 2002. Estimation of distal radius failure load with micro-finite element analysis models based on three-dimensional peripheral quantitative computed tomography images. Bone. 30, 842-48.

Radmer, S., Andresen, R., Sparmann, M., 2003. Total wrist arthroplasty in patients with rheumatoid arthritis. J Hand Surg [Am]. 28, 789–94.

Rahimtoola, Z.O., Rozing, P.M., 2003. Preliminary results of total wrist arthroplasty using the RWS Prosthesis. J Hand Surg [Br]. 28, 54–60.

Swanson, A., Matev, I., Groot, G., 1970. "The strength of the hand.," Bull Prosthet Res. 145–53.

Schuind, F., Cooney, W.P., Linscheid, R.L., An, K.N., Chao, E.Y., 1995. Force and pressure transmission through the normal wrist. A theoretical two-dimensional study in the posteroanterior plane. J Biomech. 28, 587-601.

Troy, K.L., Edwards, W.B., Bhatia, V.A., Bareither, M.L., 2013. In vivo loading model to examine bone adaptation in humans: a pilot study. J Orthop Res. 31, 1406-13.

Tajdari, M., Javadi, M., 2006. A new experimental procedure of evaluating the friction coefficient in elastic and plastic regions. J Mater Process Technol. 1, 247–50.

Ulrich, D., van Rietbergen, B., Laib, A., Rüegsegger, P., 1999. Load transfer analysis of the distal radius from in-vivo high-resolution CT-imaging. J Biomech. 32, 821-28.

Weiss, A.C., Wiedeman, G., Quenzer, D., Hanington, K.R., Hastings, H., Strickland, J.W., 1995. Upper extremity function after wrist arthrodesis. J Hand Surg [Am]. 20, 813-17.

TABLES

Table 1 - Material properties used in the FE models.

Components	Material	Elastic modulus (GPa)	Poisson's ratio
Cortical bone	Composite material	16.7	0.3
Cancellous bone	Polyurethane foam	0.155	0.3
Bone cement	PMMA	2.28	0.3
Radial-body	CoCr	210	0.3
Radial-stem	Titanium	114	0.3
Radial-head	UHMWPE	0.5	0.3

Table 2 - P-values from T-tests, performed to test the difference of mean of cortex strains between implanted and intact radius.

Load-case		Load-case 1 (abduction 15°)		Load-case 2 (neutral 0°)		Load-case 3 (adduction 45°)	
Principal Strain		ε2 (minimal)	ε1 (maximal)	ε2 (minimal)	ε1 (maximal)	ε2 (minimal)	ε1 (maximal)
Strain gauge	Dor_Dl	0.04	p<0.01	p<0.01	p<0.01	0,03	p<0.01
	Dor_Dm	0.03	p<0.01	0.03	p<0.01	0,04	p<0.01
	Dor_P	p<0.01	p<0.01	p<0.01	p<0.01	p<0.01	p<0.01
	Pal_D	p<0.01	p<0.01	p<0.01	p<0.01	p<0.01	p<0.01
	Pal_P	0.03	p<0.01	0.02	0.02	0.02	0.03
	Thu_D	p<0.01	p<0.01	p<0.01	p<0.01	0.01	p<0.01
	Thu_P	p<0.01	p<0.01	p<0.01	0.02	0.03	0.03

Table 3 - Peak values and volume of cement with von Mises stresses greater than fatigue limit, for different load cases.

Load case	Load-case 1 (abduction 15º)	Load-case 1 (neutral 0º)	Load-case 1 (adduction 45º)
von Mises peak stress (MPa)	4.31	4.05	5.67
Cement volume (%) > 6 MPa	0	0	0

LIST OF FIGURES

FIGURES

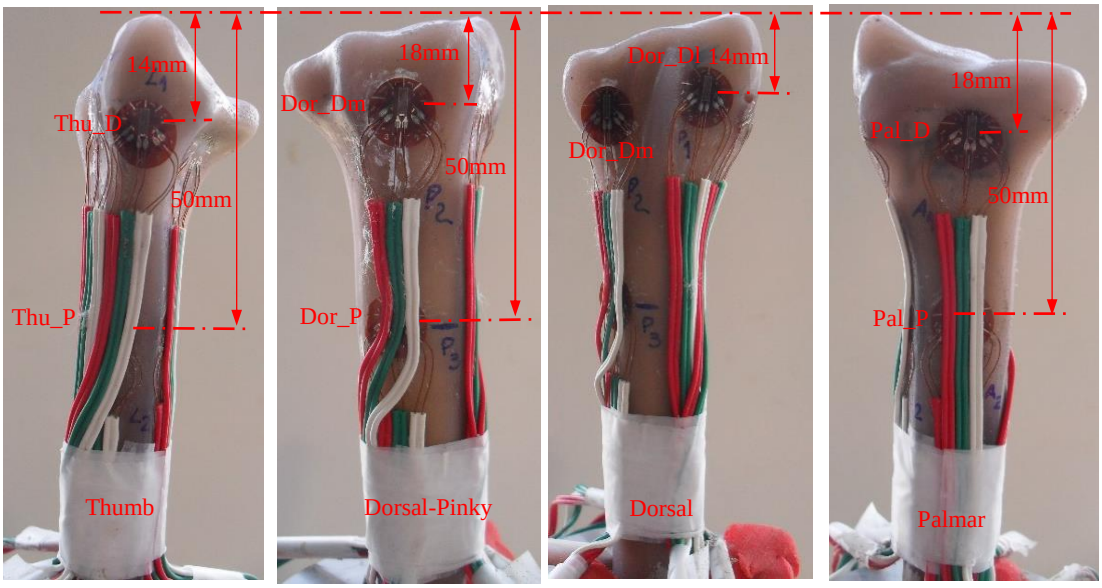

Figure 1

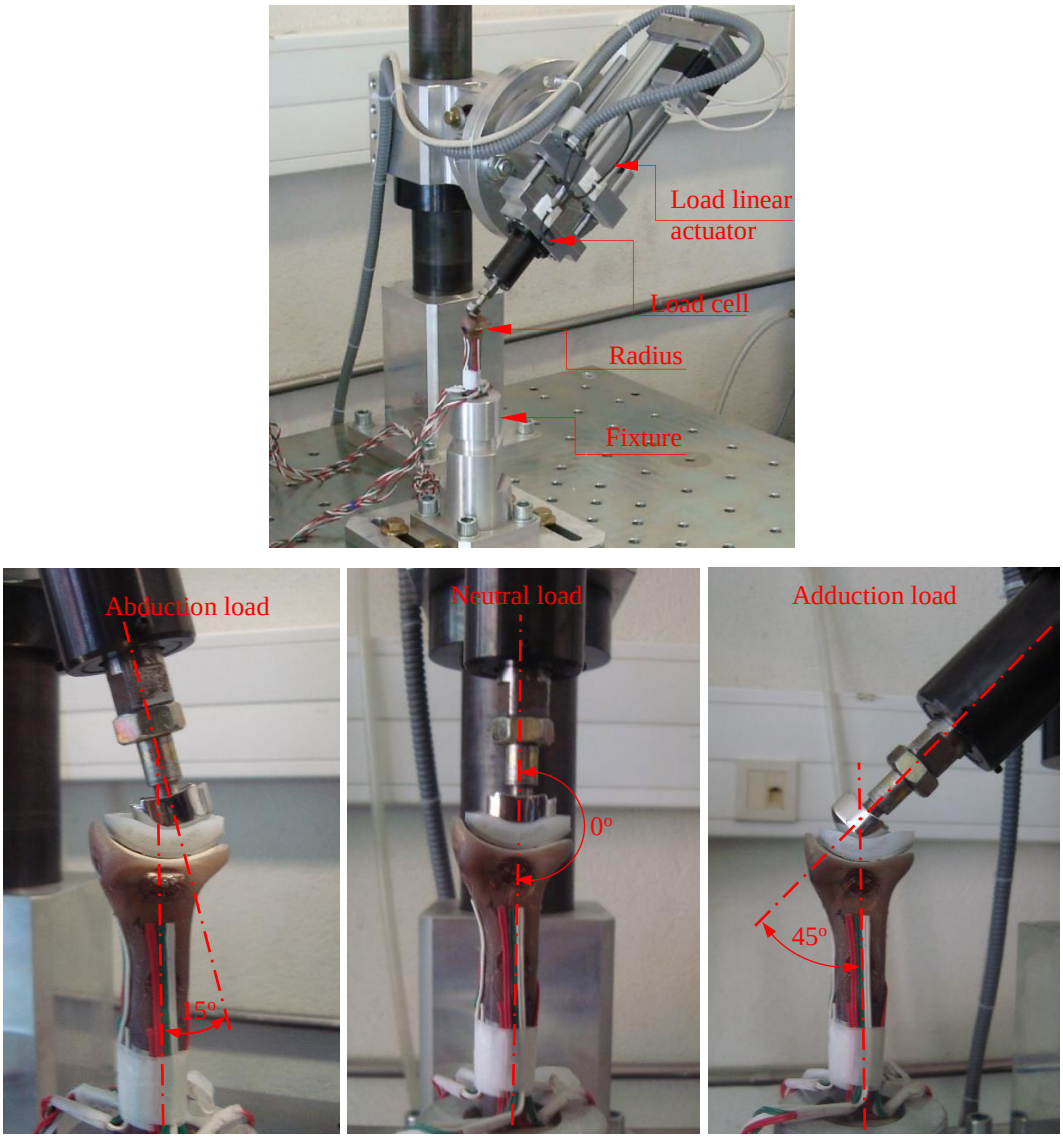

Figure 2

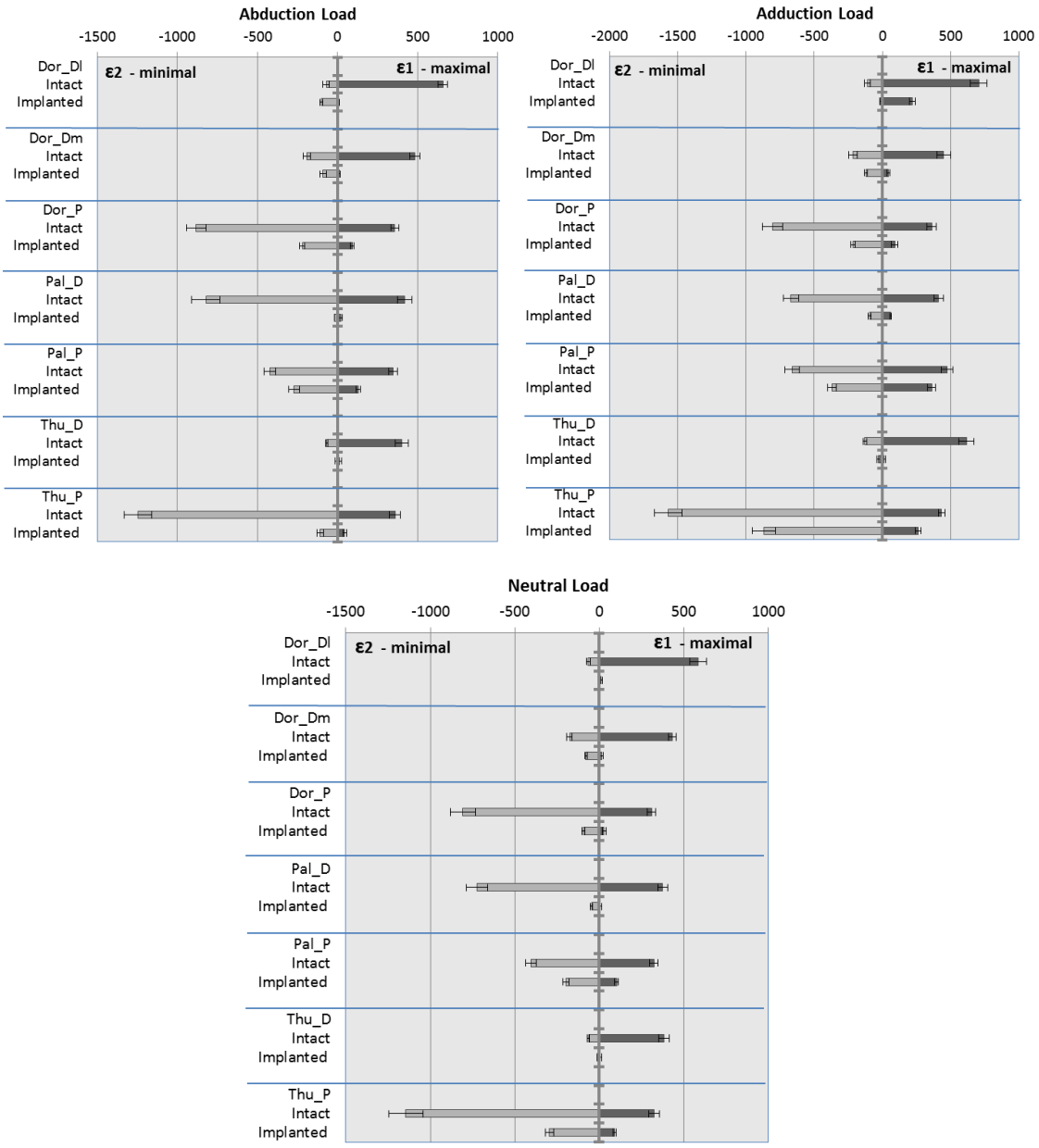
Abduction Load
-1500
-1000
-500
0
500
1000
ε2 - minimal
ε1 - maximal
Dor_Dl
Intact
Implanted
Dor_Dm
Intact
Implanted
Dor_P
Intact
Implanted
Pal_D
Intact
Implanted
Pal_P
Intact
Implanted
Thu_D
Intact
Implanted
Thu_P
Intact
Implanted
Adduction Load
-2000
-1500
-1000
-500
0
500
1000
ε2 - minimal
ε1 - maximal
Dor_Dl
Intact
Implanted
Dor_Dm
Intact
Implanted
Dor_P
Intact
Implanted
Pal_D
Intact
Implanted
Pal_P
Intact
Implanted
Thu_D
Intact
Implanted
Thu_P
Intact
Implanted
Neutral Load
-1500
-1000
-500
0
500
1000
ε2 - minimal
ε1 - maximal
Dor_Dl
Intact
Implanted
Dor_Dm
Intact
Implanted
Dor_P
Intact
Implanted
Pal_D
Intact
Implanted
Pal_P
Intact
Implanted
Thu_D
Intact
Implanted
Thu_P
Intact
Implanted

Figure 3

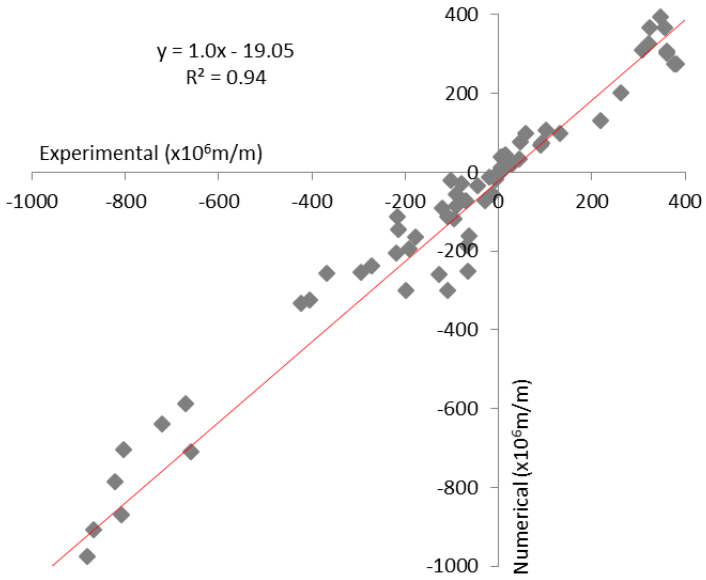
y = 1.0x - 19.05
R² = 0.94
Experimental (x10⁶m/m)
Numerical (x10⁶m/m)
400
200
0
-200
-400
-600
-800
-1000
-1000
-800
-600
-400
-200
0
200
400

Figure 4

Load case	Intact	Implanted
Adduction load 	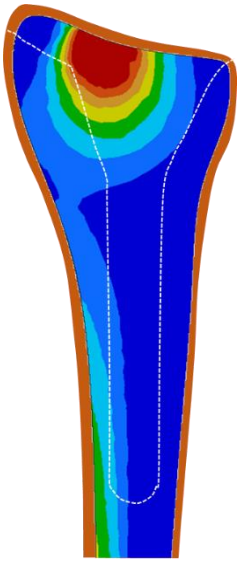	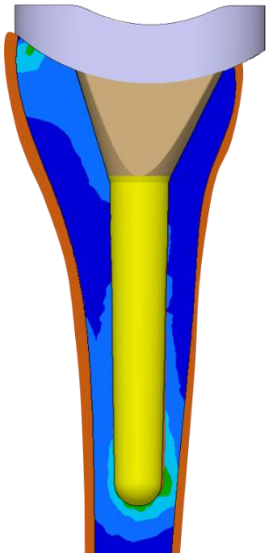
Neutral load 	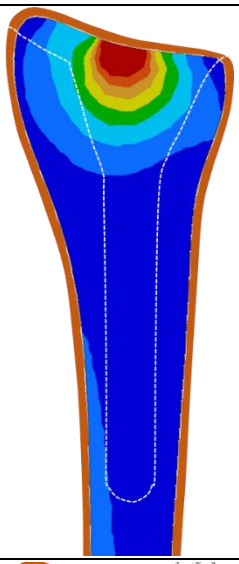	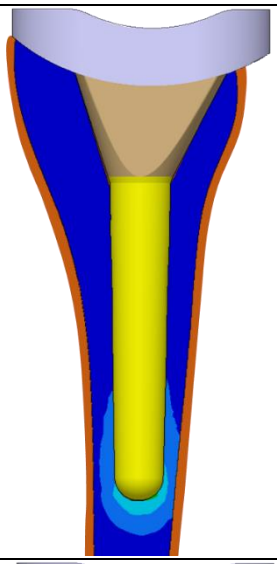
Abduction load 	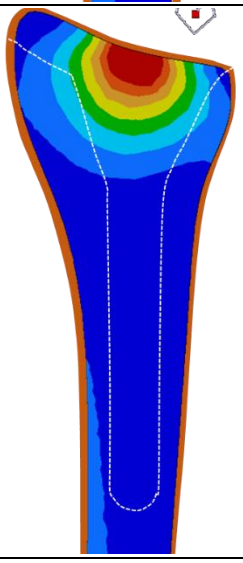	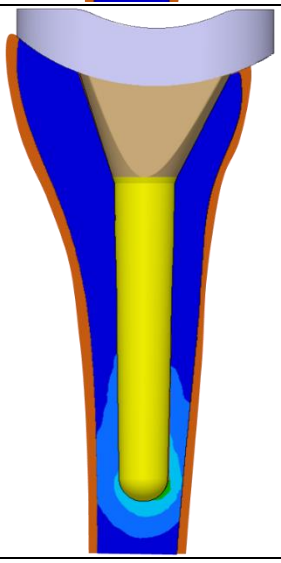

Figure 5